



Effect of Inserted Strips on Electrode Degradation in Resistance Spot Welding

Test results indicated the insertion of a Cu55Ni45 metal strip showed the most promise for extending electrode life

BY Y. Y. ZHAO, Y. S. ZHANG, X. M. LAI, AND PEI-CHUNG WANG

ABSTRACT

Recent trends toward economically fabricating lightweight vehicle structures while ensuring structural performance have led to the implementation of thin sheet steels in the automotive industry. However, one of the main challenges in resistance spot welding of ultra-thin steel (e.g., < 0.6 mm) is the extraordinarily short electrode life caused by the elevated electrode tip temperature. A method of inserting flexible strips between the electrode and workpiece has been proposed to reduce the electrode tip temperature, and consequently to prolong the electrode life.

In the present investigation, resistance spot welding of 0.4-mm-thick galvanized low-carbon steel with various inserted strips was experimentally investigated with a particular emphasis on the influence of inserted strips on the electrode degradation. Test results showed that by inserting metal strips between the electrode and workpiece, the electrode life was prolonged by about 300%. The electrode face diameter was no longer an effective indicator for the electrode degradation in resistance spot welding with inserted strips. Surface alloying and recrystallization of the material near the electrode face formed and played significant roles. Furthermore, the effects of the electro-thermal properties and compositions of the inserted strips on the electrode tip temperature and degree of surface alloying were also evaluated. Among all the strips investigated in this study, 0.12-mm-thick Cu55Ni45 metal strip exhibited the most promising results in alleviating the electrode degradation.

substrates, and thus the contact resistance at the faying interfaces accounts for larger proportion of the total joule heat generation. In other words, as the material gets thinner, the contact characteristics at the solid-solid interfaces dominate the process (Ref. 2). Since the weld size strongly relates to the contact status, it can be expected that the weldability in welding of thin-gauge steels would be poorer than that of thicker gauge. Furthermore, an extraordinarily high temperature at the electrode surface can be developed due to the rapid heat transfer from the weld zone to electrode surface when the workpieces become thinner. This excessively high temperature significantly accelerates the electrode degradation and eventually results in a reduction in electrode life by 40–60% compared to ordinary gauge sheet (Refs. 3, 4).

Recently, resistance spot welding with metal strips/cover plates/process tapes inserted between the workpiece and electrode has been adopted to join aluminum, magnesium, and ultrathin gauge steels (Refs. 3, 5–11). The inserted strip favors joule heat generation during the welding process and meanwhile shields the heat transfer from the weld zone to the electrode surface, which eventually reduces the electrode tip temperature, and consequently prolongs the electrode life (Refs. 5, 6). Kolarik successfully joined 2-mm-thick low-carbon steel to

KEYWORDS

- Resistance Welding • Thin-Gauge Steel • Automotive • Galvanized Steel

Introduction

Nowadays, light-weighting is an inevitable trend in the automotive industry. Usually, the mass reduction of vehicles is achieved either by the use of lighter, thinner, and stronger materials and/or by optimization of design throughout the vehicle structure. Thin-gauge steels might have some ad-

vantages over the use of aluminum in terms of manufacturing cost (Ref. 1). However, resistance spot welding (RSW), which is still the predominant joining technique in vehicle assembly, confronts two main difficulties in joining thin-gauge steels, especially the ones thinner than 0.6 mm. These difficulties arise from primarily two reasons. First, the decrease in steel thickness leads to lower resistance of the

Y. Y. ZHAO (Zhangyansong@sytu.edu.cn), Y. S. ZHANG, and X. M. LAI are with Shanghai Key Laboratory of Digital Manufacture for Thin-Walled Structures, Shanghai Jiao Tong University, Shanghai, PR China. PEI-CHUNG WANG is with Manufacturing Systems Research Lab, General Motors Research & Development Center, Mound Road, Warren, Mich.

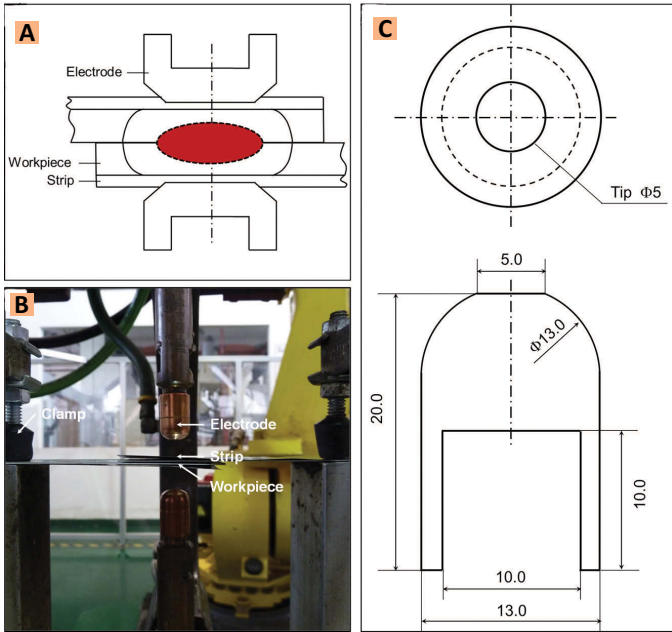


Fig. 1 — Resistance welding with inserted flexible strips. A — Schematic; B — experiment setup; C — configuration of the electrode (dimension in mm).

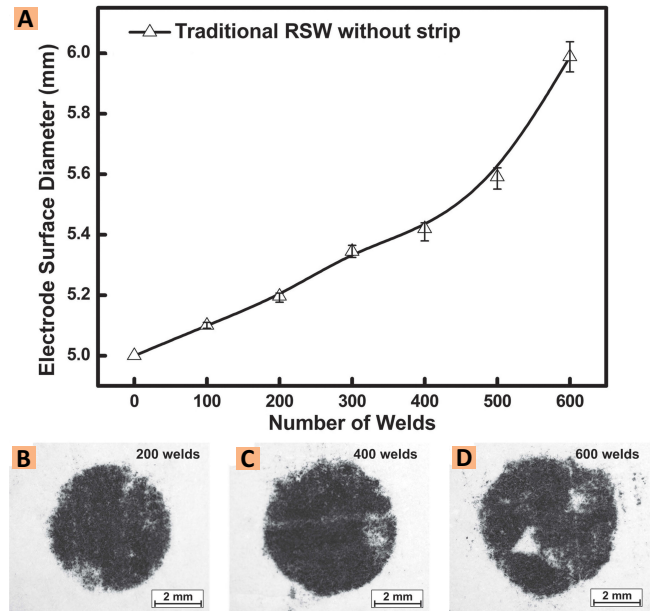


Fig. 2 — Function of number of welds during electrode wear testing of 0.4-mm-thick galvanized steel without inserted strips. A — Electrode face diameter. Carbon imprints of electrode face under the weld conditions of 1.8 kN, 5.7 kA, and 160 ms. B — After 200 welds; C — after 400 welds; D — after 600 welds.

austenitic CrNi stainless steel by using a DeltaSpot™ (Ref. 6) welding gun with a process tape (Ref. 7). Qiu and Abdo found the process tape/cover plate technique to be effective in correcting the heat imbalance and generating

heat with higher density in the aluminum side during resistance spot welding aluminum-to-steel (Refs. 8, 9). Satonaka also reported the advantages of RSW with cover plates for

joining of magnesium alloy (e.g., a comparable welding current condition to that for RSW of steel sheet) and found a weld diameter that is larger than the electrode diameter (Refs. 10, 11). Zhao investigated the effect of the inserted strips on the electrode tip temperature and weld quality during RSW of ultrathin-gauge galvanized steels and found that the effect of the inserted metal strip strongly depended on its material properties (i.e., resistivity and thermal conductivity) and thickness. With the proper selection of the metal strip, the electrode wear was reduced significantly (Ref. 3).

To date, most of the published studies focus on investigating the effect of the inserted strips on heat generation and temperature distribution, nugget formation, and joint strength, and there is little information regarding the role of the inserted strips on the microstructure evolution at the electrode surface.

The present study was undertaken to experimentally study resistance welding of 0.4-mm-thick galvanized low-carbon steel with various inserted strips. The objective of this work was to gain a better understanding of the effect of the strips on the electrode degradation from a metallurgical perspective, with a

Table 1 — Chemical Compositions (wt-%) and Mechanical Properties of Galvanized Low-Carbon Steel (DC51D+Z from Bao Steel)

Chemical Composition							Mechanical Properties			
C	Si	Mn	P	S	Fe	Coating Wt. (g/m ²)	Yield Strength (MPa)	Tensile Strength (MPa)	Elongation (%)	
0.04	0.01	0.23	0.01	0.001	balance	43–46	256	359	36	

Table 2 — Nominal Chemical Compositions of Strip Materials (wt-%)

	Cu	Cr	Ni	Zn	Mn	Fe
AISI 304	—	19	9	—	<2	balance
Cu55Ni45	balance	—	44	—	0.5–2.0	<0.5
CuNi18Zn20	balance	—	18	20	<0.7	—
Copper	>99.0	—	—	—	—	—

Table 3 — Mechanical and Electrical Properties of Strip Materials

Mechanical Properties	AISI 304	Cu55Ni45	CuNi18Zn20	Copper
Tensile strength (MPa)	505	480	450	258
Yield strength (MPa)	215	240	229	120
Elongation (%)	70	45	40	48
Modulus of elasticity (GPa)	193–200	170	133	120
Shear modulus (GPa)	86	62	49	45
Resistivity (μOhm cm)	68	55	29	2

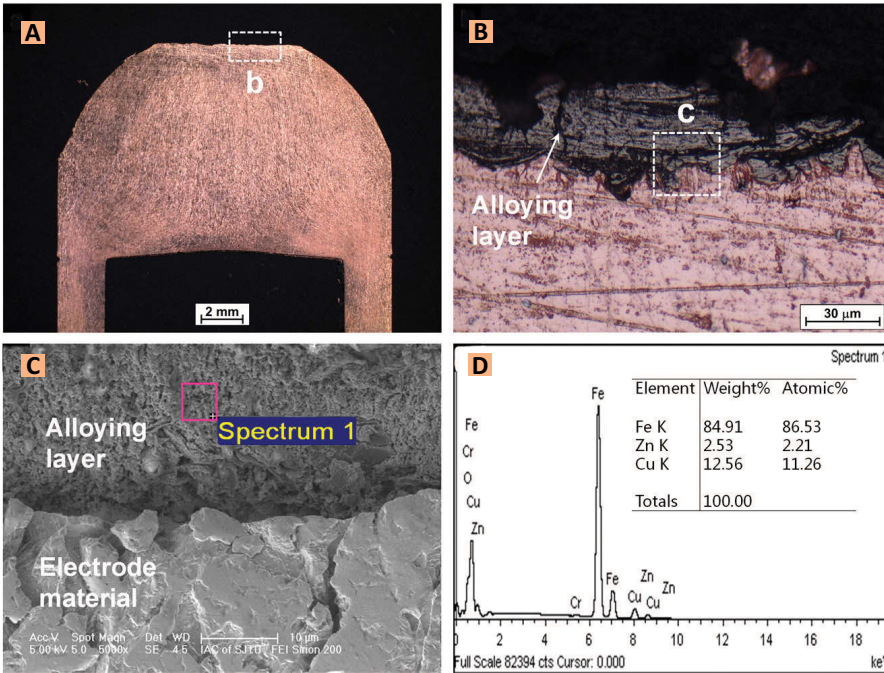


Fig. 3 — Examination of the tested electrode after 600 resistance spot welds on 0.4-mm-thick galvanized low-carbon steel without strips. A — Cross section; B — enlarged view of the dashed box in A; C — SEM of tested electrode; D — EDS scan of the alloying layer shown in square C at the electrode surface.

particular emphasis on the electrode surface alloying. The effects of the strip material, thickness, and alloy element on the electrode degradation were investigated and discussed. Finally, based on the test results, a preferable strip material for resistance welding of 0.4-mm-thick galvanized low-carbon steel was proposed.

Experimental Procedures

Materials

The steel selected in this study was 0.4-mm-thick hot-dipped galvanized low-carbon steel (i.e., DC51D+Z from Bao Steel). Per manufacturer’s data sheet, chemical compositions and mechanical properties are listed in Table 1. The metal strips used in this study are 0.05-, 0.10-, 0.15-mm-thick AISI 304 stainless steel, 0.10-mm-thick commercially available pure copper (hereinafter referred to as “copper”) and CnNi18Zn

alloy, and 0.12-mm-thick Cu55Ni45 alloy. Chemical compositions and mechanical and electrical properties of these metal strips are listed in Tables 2 and 3, respectively.

Welding Procedure

Electrode wear testing was performed using a mid-frequency DC welding machine, and the welding setup is shown in Fig. 1A. Electrodes with a 5.0-mm-diameter flat tip made of Cr-Zr-Cu alloy (compositions in wt-%: 0.2% Zr, 0.5% Cr, 0.01% Al, and the rest is Cu), shown in Fig. 1B and C, were used. Test welds were made on a 38 × 100-mm sheet of the material. The metal strips with the same size, 38 × 100 mm, were prepared. Table 4 lists the welding parameters. Electrode wear tests were conducted under a single set of welding parameters and at a welding rate of 30 welds per minute. The test was terminated once the weld size fell below the

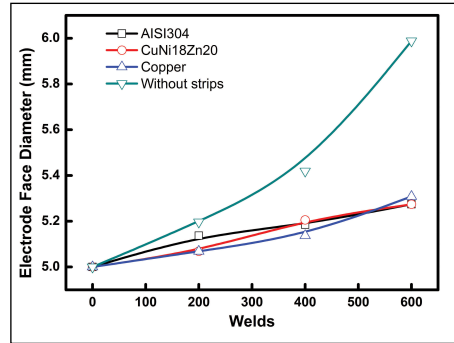


Fig. 4 — Electrode face diameter as a function of number of welds during RSW of 0.4-mm-thick galvanized steel with 0.1-mm-thick copper, CuNi18Zn20, and 304 stainless steel strips.

minimum weld nugget size (i.e., 2.5 mm of 0.4-mm thick sheet) (Ref. 12). To monitor electrode diameter and rate of electrode degradation, carbon imprints (Ref. 13) of electrode diameter were taken at the start of the electrode life test. Thereafter, imprints were taken at 100-weld increments. Peel specimens were generated at every 100-weld interval to monitor the nugget diameters. The weld nugget size was estimated by measuring the diameter of pullout buttons during the peel tests.

Microscopic Analysis

To examine the changes at the electrode face during the degradation process, cross sections of the worn electrodes were prepared and examined. The polished samples were etched in with a solution consisting of 10-g iron (III) nitrate in 100 mL of distilled water. The microstructures of the electrodes were examined by optical microscope and scanning electron microscope (SEM) equipped with Energy-Dispersive Spectroscopy (EDS) analysis. Detailed experimental parameters for SEM are listed in Table 5.

Results

Electrode life tests on RSW of 0.4-mm-thick galvanized low-carbon steel

Table 4 — Welding Parameters

Parameters	Electrode Force (kN)	Welding Current (kA)	Squeeze Time (ms)	Weld Time (ms)	Hold Time (ms)	Cooling Water Flow Rate (L/min)
Value	1.8	5.7	200	160	40	3

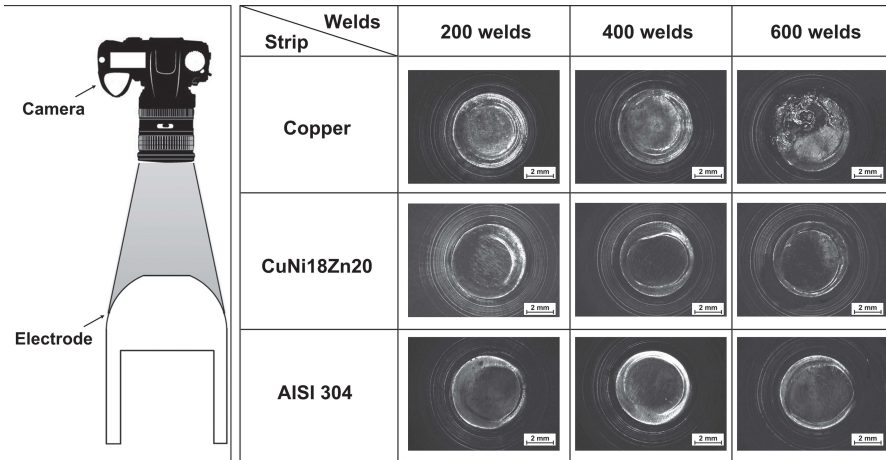


Fig. 5 — Electrode surfaces after 200, 400, and 600 welds in resistance welding of 0.4-mm-thick galvanized steel using 0.1-mm-thick copper, CuNi18Zn20, and 304 stainless steel strips.

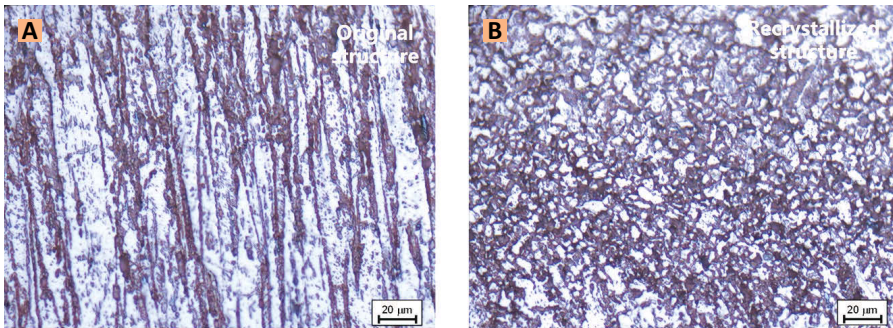


Fig. 6 — Grain structure in resistance welding of 0.4-mm-thick galvanized low-carbon steel with 0.10-mm-thick 304 stainless steel strip. A — Original copper electrode; B — recrystallized electrode.

Table 5 — Experimental Parameters for SEM

Parameters	Accelerating Voltage (kV)	Spot Size (nm)	Detectors	Working Distance (mm)
Value	5.00	4/5	SE	4.5~5.5

without and with various inserted strips were conducted. There are three main parts in the test results. First, the electrode degradation process without inserted strip was evaluated. This was followed by assessing the effects of resistivity and thickness of the inserted strip on the electrode life. Finally, we discuss the combined effects of resistivity, thickness, and alloy content of the inserted strip on the electrode degradation.

Electrode Degradation in RSW of Ultrathin Steel

Electrode life tests on RSW of 0.4-

mm-thick galvanized low-carbon steel without inserted strips were terminated after 600 welds because the weld size decreased to 2.4 mm, which is below the minimum acceptable size of 2.5 mm (Ref. 12). Figure 2A presents the measured face diameters as a function of weld number. As shown, electrode face diameter increased from 5 to 6 mm after 600 continuous welds. The imprints of the electrode face after 200, 400, and 600 welds are shown in Fig. 2B, C, and D, respectively. Careful examinations of the worn electrodes with 600 welds, shown in Fig. 2D, indicated that severe cavitation developed at the electrode face. These results suggest that the electrodes had

degraded significantly.

Microscopic examinations of the worn electrodes after 600 welds were performed and the results are shown in Fig. 3. As shown in Fig. 3A, the cross section of the worn electrodes exhibited a rough surface profile. After etching, a dark layer, about 25~30 μm thick, was revealed at the electrode surface, shown in Fig. 3B and C. EDS analysis of the region labeled by a square in Fig. 3C was performed and the results are presented in Fig. 3D. As shown, the layer contains about 86% iron, 11% copper, and 2% zinc (at.-%). Compared to the compositions of the as-received electrode material (i.e., 0.2% Zr, 0.5% Cr, 0.01% Al, and the rest Cu), the difference in composition is primarily caused by the sticking of workpiece and zinc coating onto the electrode surface under the high temperature and the exertion of electrode force. Formation of this alloy layer and its high iron content indicated that severe electrode degradation occurred.

Electrode Degradation in RSW of Ultrathin Steel with Inserted Strip

To minimize the electrode degradation, a metal strip was introduced in between the electrode and workpiece. It has been reported that the presence of strip material strongly affected the heat generation and temperature distribution during the welding process (Ref. 3). In this study, three strip materials (i.e., commercially pure copper, CuNi18Zn20 alloy, and 304 stainless steel strips) that have lower, comparable, and higher electrical resistivity than that of the workpieces were selected to assess their influences on the growth of electrode face diameter, recrystallization, and surface alloying of copper electrode. To study the influence of the strip materials on the electrode degradation process, the thickness of these strips was fixed at 0.10 mm.

Electrode Face Diameter

Electrode life testing was performed, and the weld size was still acceptable after 2000 welds by making use of the inserted strips. Compared to the electrode life of 600 welds in welding without

strips, it was prolonged by about 300% with using inserted strips.

The growth of electrode face diameter has been commonly used to assess the extent of the electrode degradation (Ref. 13). The changes in electrode face diameter are shown in Fig. 4. For the purpose of comparison, test results for the case without the strip are also included. As shown in Fig. 4, all electrode face diameters increased with increasing number of welds and reached a face diameter of about 5.3 mm after 600 welds. Electrode face diameter for the case without a strip is larger than those with the presence of the strips by ~0.7 mm. The strip materials used in this study had little influence on the electrode face diameter. To understand the effect of strip material on the electrode degradation mechanism, the appearances of the worn electrodes were analyzed.

Figure 5 presents the effect of the strip material on the electrode appearances after 200, 400, and 600 continuous welds for copper, CuNi18Zn20, and 304 strips. As shown, except the electrodes used with copper strip, all electrode faces exhibited little pitting or cavitation and mushrooming after 600 welds. Previous studies suggested that a number of different damage processes developed during the degradation of electrodes when welding zinc-coated steel, namely: recrystallization of the electrode material, mushrooming or growth of electrode face, and surface alloying and pitting/cavitation (Ref. 14). However, careful examinations of the worn electrodes indicated that this is not what we have observed in RSW of thin steel with inserted strips. Test results indicated that in RSW of thin steel with inserted strips, the most prominent change in the electrode face was that a convex surface was formed at the center and expanded toward the edge. Since there is little difference in electrode face diameter, the worn electrodes

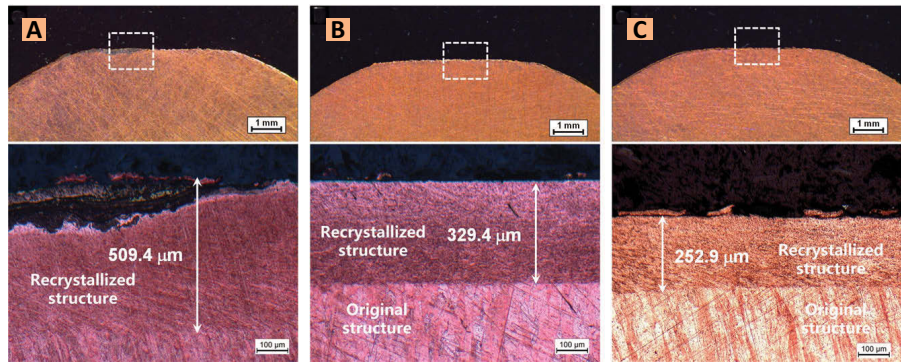


Fig. 7 — Effect of 0.10-mm strip material on the electrodes after 600 continuous resistance spot welds on 0.4-mm-thick galvanized low-carbon steel. A — Copper strip; B — CuNi18Zn20 strip; C — 304 stainless steel strip.

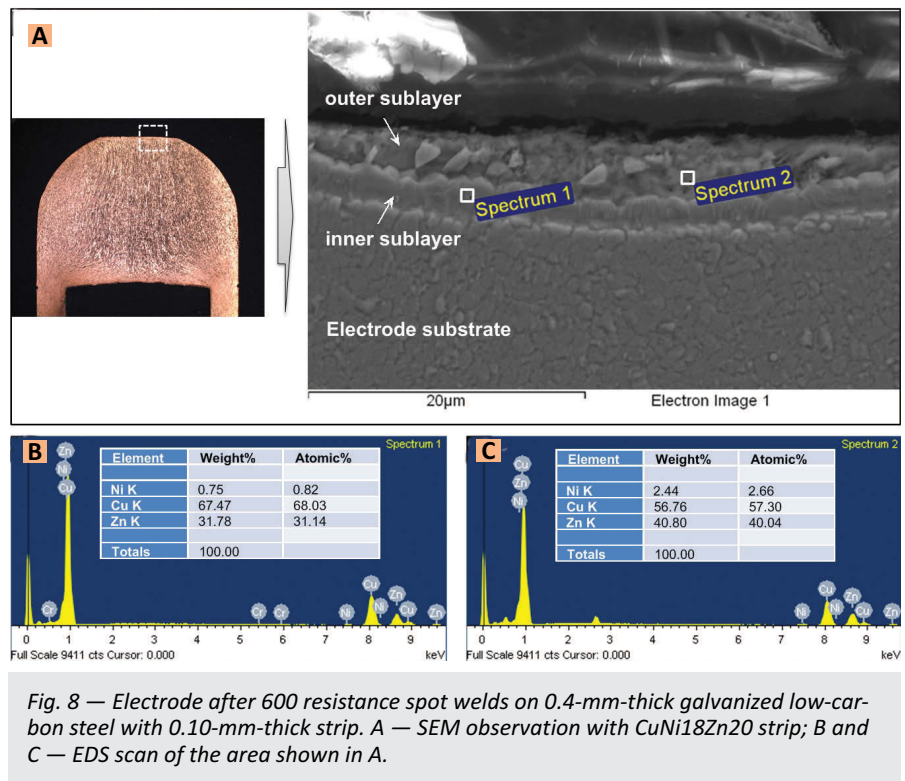


Fig. 8 — Electrode after 600 resistance spot welds on 0.4-mm-thick galvanized low-carbon steel with 0.10-mm-thick strip. A — SEM observation with CuNi18Zn20 strip; B and C — EDS scan of the area shown in A.

were cross-sectioned and examined microscopically to see if they were recrystallized and surface alloyed during the welding process. Test results are described next.

Recrystallization of Electrode Material

Published results (Refs. 15, 16) showed that recrystallization of the electrode below the electrode surface

Table 6 — Effect of Strips on the Recrystallization and Surface Alloying of the Electrode in RSW of 0.4-mm-thick Galvanized Low-Carbon Steel

Material	Strip Thickness (mm)	Recrystallization Layer (μm)	Surface Alloy Layer	
			Thickness (μm)	Composition (at.-%)
AISI 304	0.05	—	—	—
	0.10	252.9	6	87% Cu, 7% Fe, 6% Ni
	0.15	435.3	10	81% Cu, 16% Fe, 1.5% Ni
Copper	0.10	509.4	>100	
	0.10	329.4	6.5	inner: 68% Cu, 31% Zn, 1% Ni outer: 57% Cu, 40% Zn, 3% Ni
Cu55Ni45	0.12	94.1	2	92% Cu, 8% Ni

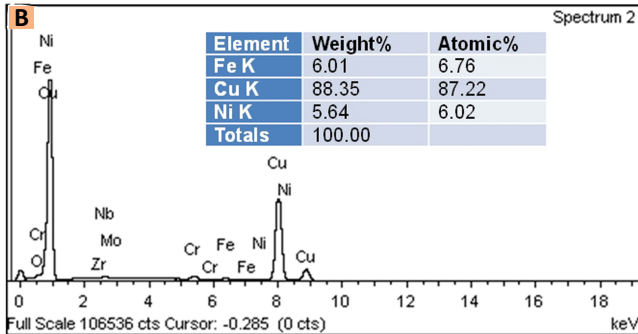
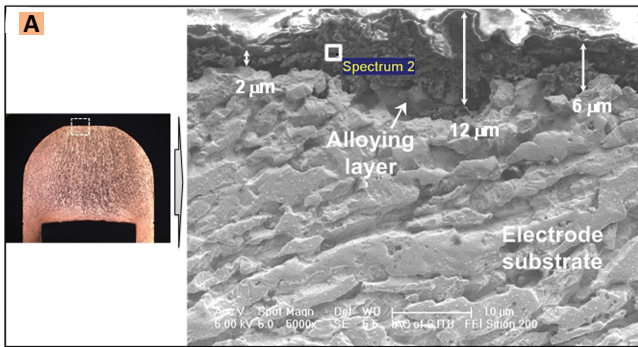


Fig. 9 — Electrode after 600 resistance spot welds on 0.4-mm-thick galvanized low-carbon steel with 0.10-mm-thick strip. A — SEM with 304 stainless steel strip; B — EDS scan of the square shown in A.

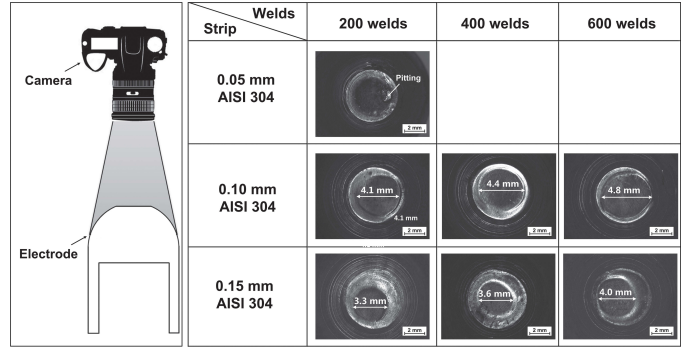


Fig. 10 — Effect of the thickness of 304 stainless steel strip on the electrode degradation in resistance welding of 0.4-mm-thick galvanized low-carbon steel.

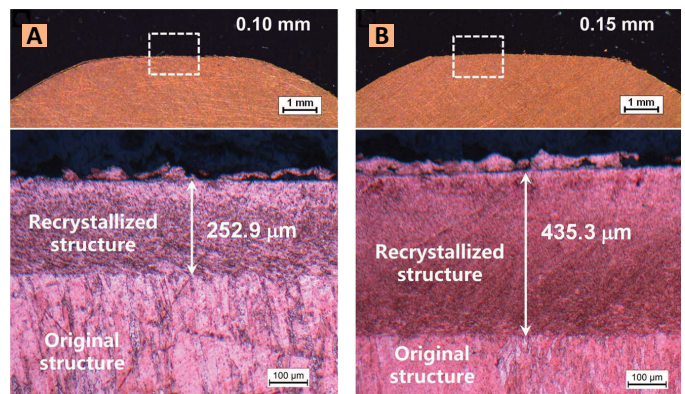


Fig. 11 — Effect of strip thickness on the recrystallization of the electrode surface after 600 continuous resistance spot welds on 0.4-mm-thick galvanized low-carbon steel with the presence of 304 strips. A — 0.10 mm thick; B — 0.15 mm thick.

frequently occurred due to high temperature, and it is usually accompanied by a marked reduction in the strength and hardness of the material. It was reported that a decrease in hardness from 176 to 70–90 HV occurred within the recrystallized zone (Ref. 4). Since electrode softening is one of the dominant damage processes, the depth of recrystallization layer could be an effective indication of electrode degradation. Once recrystallization occurred, a pronounced change in grain structure was observed. Figure 6A and B present the microstructures of the as-received and copper electrodes after 600 welds in resistance welding of 0.4-mm-thick galvanized low-carbon steel with 0.10-mm-thick 304 strip, respectively. As shown, while as-received copper electrode consisted of elongated grains, the recrystallized regions of the worn electrode were composed of primarily fine grains.

Due to this difference in microstructures of as-received and recrystallized electrodes, the thickness of the recrystallized layer of the worn electrodes was examined. Figure 7A, B, and C shows the recrystallized layers for copper, CuNi18Zn20, and 304 stainless steel strips, respectively. As shown, while the thickness of the re-

crystallized layer is more than ~500 μm with a 0.1-mm-thick copper strip, it reduced to ~330 and ~250 μm for the 0.1-mm-thick CuNi18Zn20 and 0.1-mm-thick AISI 304 strips, respectively. These results inferred that the electrode tip temperature with CuNi18Zn20 strip is likely lower than that with copper strip but higher than that with 304 stainless strip.

Surface Alloying

During resistance welding, surface coatings often alloy with the electrode material due to the high temperature experienced at the electrode surface. This alloying makes a significant contribution to the overall electrode damage process (Ref. 4). To assess if the surface alloying would form with the presence of metal strips, SEM and EDS were employed to investigate the microstructure and chemical compositions of the alloying layer on the electrode surface and the results are shown in Figs. 8 and 9.

As shown in Fig. 8A, a ~6.5-μm-

thick alloying layer on the electrode surface after 600 welds in RSW of 0.4-mm-thick galvanized low-carbon steel with the presence of CuNi18Zn20 strip was formed. As shown, this alloying layer was composed of two sublayers. EDS analysis results of these sublayers shown in Fig. 8B and C revealed that they mainly contained copper, zinc, and a trace of nickel. These results suggest that zinc in the strip is most likely to alloy with the copper electrode due to its lower melting point and higher chemical activity compared to nickel and copper.

Similar analyses were conducted on the worn electrodes with the use of 304 stainless steel strip and the results are shown in Fig. 9. As shown in Fig. 9A, the alloying layer with the use of 304 strip had a thickness of ~6.6 μm, which is close to that (i.e., 6.5 μm thick) of using CuNi18Zn20 strip. However, the copper content in the alloying layer with 304 strip is (~ 87%)

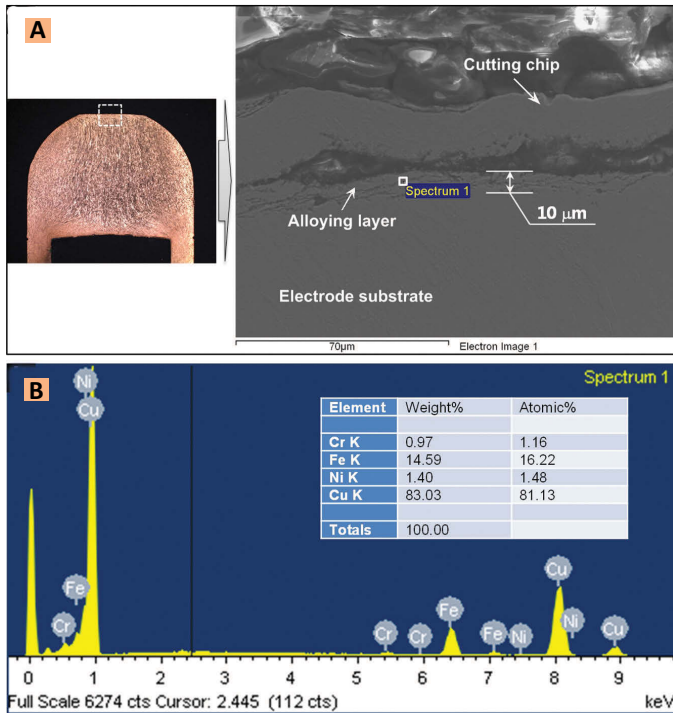


Fig. 12 — Electrode after 600 resistance spot welds on 0.4-mm-thick galvanized low-carbon steel with 0.15-mm-thick 304 stainless steel. A — SEM observation; B — EDS scan of the region shown in the square in A.

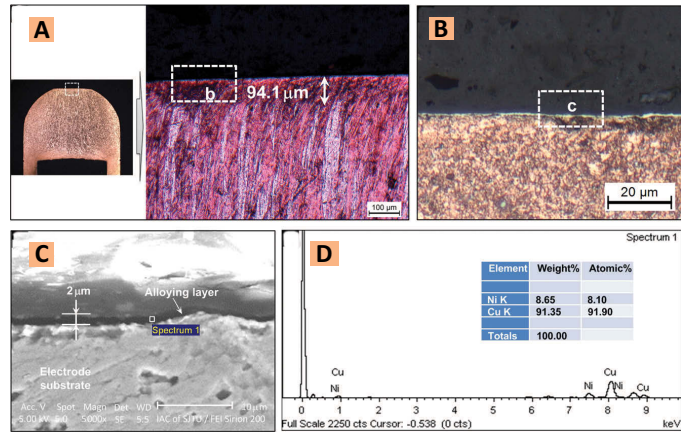


Fig. 13 — Resistance spot weld on 0.4-mm-thick galvanized low-carbon steel with 0.12-mm-thick Cu55Ni45 alloy strips after 600 welds. A, B — Optical observation; C — SEM observation of the electrode; D — EDS scan of the alloying layer.

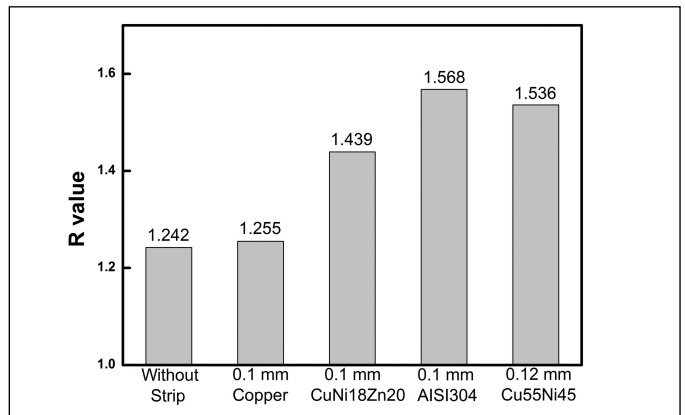


Fig. 14 — Calculated R value of different strips in resistance spot welding of ultrathin gauge steel.

far higher than that with CuNi18Zn20 strip. Therefore, although the thicknesses of the alloying layers are similar with these two strips, the higher copper content in the alloying layer with 304 strip indicates a lower extent of surface alloying.

Based on the aforementioned results, we can conclude that pure copper is a less desirable choice than 304 steel and CuNi18Zn20 because of its extraordinary high thermal conductivity. Moreover, a suitable strip should not contain Zn, owing to its low melting point and active chemical property. Desired strips incline to be copper-nickel based alloy and stainless steel. Within the selected strips studied here, due to the lowest degree of electrode recrystallization and the highest content of copper in the alloying layer formed at the electrode surface by making use of 304 strips, 304 stainless steel had the most promising performance in lowering electrode temperature and alleviating electrode degradation.

Effect of Strip Thickness

After 304 stainless steel was identified as the preferred strip material, the

effect of its thickness on the electrode wear and surface alloying was examined next. The 304 stainless steel with the thicknesses of 0.05, 0.10, and 0.15 mm was selected. Figure 10 presents the effect of the thickness of 304 stainless steel strip on the changes to the electrode surface. As shown, due to severe pitting occurring at the electrode surface using a 0.05-mm-thick 304 strip, tests were terminated after 200 welds. Since a 0.05-mm-thick strip is quite thin, the asperities on the electrode face or workpieces occasionally perforated through the strip under the exertion of electrode force and led to extreme current concentration, and consequently resulted in severe surface expulsion and severe pitting on the electrode surface. For 0.10- and 0.15-mm-thick strips, a convex surface was formed at the center of the electrode and expanded toward the edge. Comparisons of the worn electrodes shown in Fig. 10 indicated that the difference resulting from

using these two strip thicknesses was the diameter of the convexity being smaller for the thicker strip. Increased stiffness of the thicker strip led to a smaller contact radius at the electrode/strip and strip/workpiece interfaces, which further resulted in the concentration of current density and heat generation at the contacting area. Therefore, the size of the convexity became smaller using thicker strips. Moreover, the worn electrodes were examined to assess the degree of recrystallization and surface alloying.

Figure 11A and B shows the cross sections of the electrodes with 0.10- and 0.15-mm-thick 304 strip after 600 continuous welds, respectively. As shown, recrystallized grains were formed beneath the electrode face. While the thickness of the recrystallized layer was ~250 μm with a 0.10-

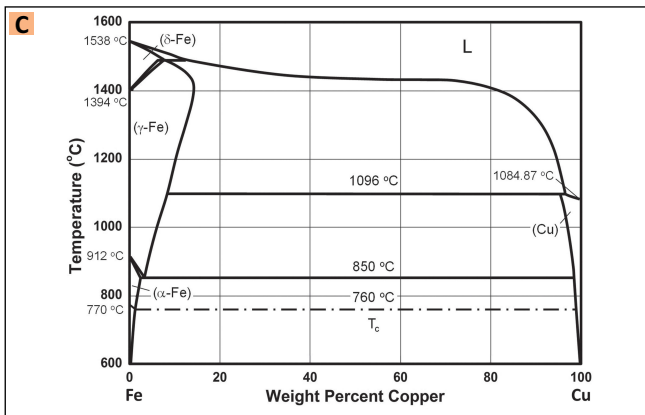
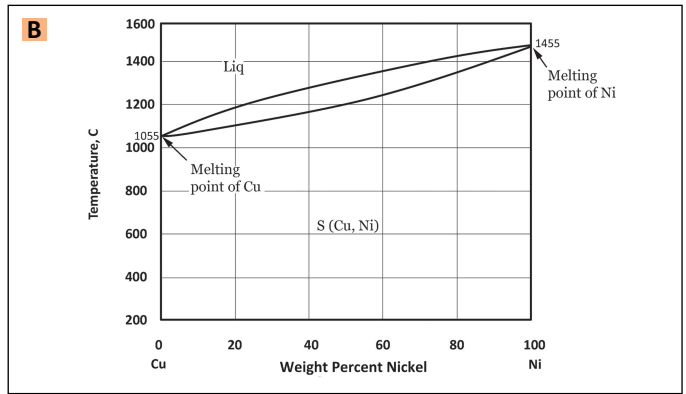
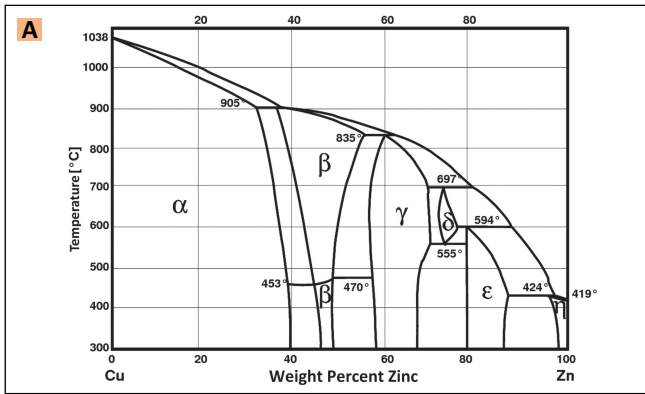


Fig. 15 — Binary phase diagrams (Ref. 20). A — Cu-Zn; B — Cu-Ni; C — Cu-Fe.

mm-thick 304 strip, it increased to ~435 μm when the strip was thickened to 0.15 mm. These results suggested that the temperature at the electrode face with a 0.15-mm-thick strip is higher than that with a 0.10-mm-thick strip. Thicker strip possesses higher electrical bulk resistance, and therefore is more favorable to heat generation and especially since the resistivity of 304 stainless steel is much higher than that of steel sheets. Therefore, a higher temperature would develop at the electrode face with thicker 304 stainless steel strips.

SEM and EDS analysis results of the worn electrodes after 600 welds in RSW of 0.4-mm-thick galvanized low-carbon steel with 0.15-mm-thick 304 steel, shown in Fig. 12, further validated the above results. After etching, a 10- μm -thick alloying layer emerged loosely at the electrode surface. This alloying layer contained ~81% copper, ~16% iron, and traces of Ni and Cr (at.-%). Comparing the results shown in Figs. 9B and 12B indicates that the iron content in the alloying layer increased from ~7 to ~16% with an increase in thickness to the 304 strip from 0.10 to 0.15 mm, which suggested a higher degree of surface alloying.

shown above indicated that 0.10-mm-thick 304 stainless steel strip is more favorable than 0.15-mm-thick 304 strip to prolong the electrode life in RSW of 0.4-mm-thick galvanized low-carbon steel.

Comparison of Strip Material

The aforementioned results of effect of strip material on electrode wear indicated that the desired strips incline to be copper-nickel alloy and stainless steel. Therefore, it would be interesting to compare copper-nickel alloy strip to 304 stainless steel. To make a fair comparison, Cu55Ni45 was selected because its mechanical properties are similar to that of 304. The thickness of Cu55Ni45 alloy strip was determined as 0.12 mm to ensure that its electrical resistance is comparable to that of 0.10-mm-thick 304 steel strip (i.e., resistivities of 304 steel and Cu55Ni45 are 68 and 55 $\mu\text{Ohm/cm}$, respectively). Electrode life tests were conducted and Fig. 13A and B presents the cross sections of the worn electrode after 600 continuous RSW of 0.4-mm-thick galvanized low-carbon steel with the presence of a

0.12-mm-thick Cu55Ni45 strip. As shown, a layer of recrystallized grains with ~100- μm -thickness was observed in the area near the electrode surface, which was far thinner than that (~250 μm) of the electrodes with a 0.1-mm-thick 304 strip. Besides, the thickness of the alloying layer shown in Fig. 13C at the electrode surface decreased to ~2 μm . EDS analysis results of the alloying layer shown in Fig. 13D revealed that the composition of the layer is 91.9% Cu and the rest is Ni. All these results indicated a lower extent of electrode degradation with 0.12-mm-thick Cu55Ni45 strip.

To sum up all the test results presented above, Table 6 lists the effect of all strips used in this study on the recrystallization and surface alloying in resistance welding of 0.4-mm-thick galvanized low-carbon steel. It can be seen that the thicknesses of recrystallized and alloying layers were the thinnest, and the alloying layer contained also the highest copper content (~92%) with the 0.12-mm-thick Cu55Ni45 strip among all strips selected in this study. These results suggested that 0.12-mm-thick Cu55Ni45 is the most desired strip choice. And yet for all that, 0.10-mm 304 stainless steel exhibited the second-least electrode wear.

Discussions

Electrode Tip Temperature

Experimental results showed that the extent of the electrode degradation with the presence of a metal strip was quite different from that without the metal strip in resistance welding of 0.4-

mm-thick galvanized low-carbon steel. The effect of the inserted strips on the electrode tip temperature can be explained from two aspects. One is “heating effect” caused by the resistance of the strip itself and contact resistance of additional faying interfaces, and the other is “insulation effect” that the strip acts as a heat shield between the workpiece and electrode to insulate heat transfer from the weld zone to the copper electrode. Since it is difficult to measure the electrode tip temperature experimentally, an analytical model (Refs. 17, 18) was employed here to estimate the electrode tip temperature and analyze the effects of metal strip and its properties on the temperature at the electrode-to-workpiece interface. This analytical analysis has the following assumptions:

- 1) Heat flow from the workpiece into the electrodes is simplified to one dimension.
- 2) The peak temperature distribution in the resistance spot weld can be described by a sine wave half period, with the peak at the faying interface of the workpieces.
- 3) It is assumed that the thermal gradient in the electrode is linear, extending from electrode tip temperature Θ_E to the temperature of the cooling water (assumed to be room temperature for this analysis).
- 4) Thermal gradient in the strip is linear as well, extending from electrode tip temperature Θ_E to temperature strip/workpiece interface temperature Θ_S .
- 5) The top and bottom electrodes are essentially straight sided.

The function of temperature distribution in the workpiece and boundary condition can be summarized as

$$\left\{ \begin{array}{l} \Theta = (\Theta_P - \Theta_S) \cos\left(\frac{\pi}{2\Delta x} x\right) + \Theta_S; \\ \text{temperature distribution in workpiece} \\ \frac{d\Theta}{dx} x = \Delta x_{Strip} = -\frac{k_E}{k_{Strip}} \frac{\Theta_E}{\Delta x_E}; \\ \text{boundary condition at electrode /} \\ \text{strip interface} \\ \frac{d\Theta}{dx} x = \Delta x = -\frac{k_{Strip}}{k_S} \frac{(\Theta_S - \Theta_E)}{\Delta x_{Strip}}; \\ \text{boundary condition at workpiece /} \\ \text{strip interface} \end{array} \right. \quad (1)$$

where Θ_P is the peak temperature in the spot weld, Δx is the thickness of the workpiece, Δx_E is the electrode face thickness (i.e., distance between the face and underside of the electrode), k_E and k_S are the thermal conductivities of the electrode material (Cu) and workpiece, respectively, and x is the distance from the weld faying surface toward the electrode face. k_{Strip} and Δx_{Strip} are the thermal conductivity and thickness of the inserted strip, respectively, and Θ_S is the temperature at the workpiece/strip interface. Combining the function of temperature distribution and boundary conditions (i.e., in Equation 1), and then, the Θ_E of RSW with the inserted strip can be estimated as

$$\Theta_E = \frac{\Theta_P}{1 + \left(\frac{k_E}{k_{Strip}}\right) \left(\frac{\Delta x_{Strip}}{\Delta x_E}\right) + \left(\frac{2}{\pi}\right) \left(\frac{k_E}{k_S}\right) \left(\frac{\Delta x_S}{\Delta x_E}\right)} \quad (2)$$

In sum, the temperature developed at the electrode surface Θ_E can be expressed as

$$\Theta_E = \begin{cases} \frac{\Theta_P}{1 + \left(\frac{2}{\pi}\right) \left(\frac{k_E}{k_S}\right) \left(\frac{\Delta x}{\Delta x_E}\right)}; \\ \text{traditional RSW (Refs. 17, 18)} \\ \frac{\Theta_P}{1 + \left(\frac{k_E}{k_{Strip}}\right) \left(\frac{\Delta x_{Strip}}{\Delta x_E}\right) + \left(\frac{2}{\pi}\right) \left(\frac{k_E}{k_S}\right) \left(\frac{\Delta x_S}{\Delta x_E}\right)}; \\ \text{RSW with strips} \end{cases} \quad (3)$$

To define an R for the ratio of Θ_P/Θ_E , Equation 3 can be rewritten as

$$R = \frac{\Theta_P}{\Theta_E} = \begin{cases} 1 + \left(\frac{2}{\pi}\right) \left(\frac{k_E}{k_S}\right) \left(\frac{\Delta x}{\Delta x_E}\right); & \text{traditional RSW} \\ 1 + \left(\frac{k_E}{k_{Strip}}\right) \left(\frac{\Delta x_{Strip}}{\Delta x_E}\right) + \left(\frac{2}{\pi}\right) \left(\frac{k_E}{k_S}\right) \left(\frac{\Delta x_S}{\Delta x_E}\right); & \text{RSW with strips} \end{cases} \quad (4)$$

The ratio R can quantitatively evaluate the “insulation effect” of the inserted strips, and a greater R value indicates the lower electrode tip temperature if the value of Θ_P is constant. Plugging the material properties (Ref. 19) into Equation 4, the calculated results are shown in Fig. 14.

As shown, the temperature ratio R increases with the presence of the strips. For a given sheet stack-up, the calculated R value with copper strip is

slightly greater than that without strip. These results suggest that the joule heat generated at the weld zone can readily transfer through the copper strip to the electrode surface, and consequently result in high electrode tip temperature. The calculated R values for 0.1-mm-thick 304 and 0.12-mm-thick Cu55Ni45 strips are the two highest, and consequently lower electrode tip temperature can be expected. Test results showed that the electrode wear with 0.12-mm-thick Cu55Ni45 was less than that with 0.1-mm-thick 304, shown in Table 3, even though the R value with 0.1-mm-thick 304 is greater than that with 0.12-mm-thick Cu55Ni45. This disagreement likely is attributed to two reasons. First, it is difficult to estimate Θ_P quantitatively by the analytical method due to a series of assumptions and simplifications made in the formulations. Furthermore, temperature is not the only factor affecting the electrode wear; metallurgical factor is another important aspect and will be discussed in the section below.

Alloying Element

In this part, the alloying compounds formed between the electrode and inserted strips and their influences on the hardness and electrical properties of the copper electrode are discussed by referring to binary phase diagrams. To explain the effect of CuNi18Zn20 strip on the electrode wear protection, the Cu-Zn binary phase diagram shown in Fig. 15A is referred to. As shown, there are several intermetallic compounds (IMC) (e.g., α phase Cu3Zn and Cu9Zn solid solution, β phase CuZn base solid solution, and γ phase Cu5Zn8 base solid solution) formed. With the presence of CuNi18Zn20 strips, as shown in Fig. 8, the alloying compounds contained two sublayers that had 40 and 30% zinc, respectively. Based on EDS analysis results of the composition in the alloying layer shown in Fig. 8 and the Cu-Zn phase diagram, the outer layer should be $\alpha + \beta$ phase while the inner layer is composed of α phase. Because β phase IMC is quite soft (Ref. 20), it is unfavorable for the electrode performance.

To assess Cu-Ni alloying compounds, see the Cu-Ni phase diagram in Fig. 15B. As shown, Cu and Ni elements are completely soluble in each other and

form a continuous solid solution. Thus, the alloying compounds would be a Cu-Ni solid solution with different proportions of the two elements. Similar analysis was performed for Cu-Fe alloying compounds with the Cu-Fe phase diagram shown in Fig. 15C. As shown, the solid solubility of iron in copper or copper in iron is extremely low (i.e., <2%), and there is no intermediate phase formed between Cu-Fe. Therefore, Cu-Fe alloy with various components is all made of the mixture of solid solutions at both ends. In sum, Cu-Ni and Cu-Fe systems are not likely to form intermetallic compounds, and therefore, the surface alloying layer would affect little the hardness of the copper electrode.

Published results (Ref. 21) indicated that the alloying element in copper-based solid solution exerted a significant influence on the electrical conductivity. Due to the extraordinary electrical conductivity of pure copper, addition of almost all other elements into copper would lead to a decrease in electrical conductivity. It is noted that addition of Fe into copper caused a dramatic decrease in electrical conductivity (Ref. 21). Therefore, Fe-rich alloying layer deposited at the electrode surface would significantly increase the electrical resistance at the electrode surface, and consequently enhance the joule heating, which would further exacerbate the electrode degradation. Therefore, considering the effect of alloying on the electrical characteristics of copper electrode, an alloying product between Cu-Ni alloy strip and the electrode provides the least impact on the hardness and electrical conductivity of the electrode. This is consistent with the experimental observations in this study.

Conclusions

1) The presence of inserted metal strips alleviated the extent and rate of electrode degradation in resistance spot welding of 0.4-mm-thick galvanized low-carbon steel. The process of electrode degradation was different from that of traditional resistance spot welding. Alloying and recrystallization still occurred at the electrode surface, but the growth in electrode surface diameter was significantly reduced.

2) The effects of the electrothermal

properties of the strips on the electrode tip temperature and surface alloying were analyzed. Strips with comparatively higher electrical resistivity (e.g., 304 stainless steel and Cu55Ni45) lowered the electrode tip temperature compared to the strips with higher thermal/electrical conductivity (e.g., commercially pure copper).

3) Analysis of the effect of the strip compositions on the electrode surface alloying revealed that the alloying compounds produced with the introduction of Cu-Ni alloy strip had the least impact on the hardness/strength and electrical conductivity of a copper electrode.

4) Among all strips investigated in this study, 0.12-mm-thick Cu55Ni45 alloy strip provided the best protection of the electrode degradation in resistance welding of 0.4-mm-thick galvanized low-carbon steel.

Acknowledgments

This research was supported by the General Motors Collaborative Research Laboratory at Shanghai Jiao Tong University. This research was also sponsored by Shanghai Rising-Star Program (11QA1403600) and Project 51275304 supported by National Natural Science Foundation of China.

References

1. Pecas, P., Henrique, M., Miranda, R. M., and Quintino, L. 1995. Laser welding of low-thickness zinc-coated and uncoated carbon steel sheets. *Optical and Quantum Electronics* 27(12): 1193–1201.
2. Calva, C. M., and Eagar, T. W. 1990. Enhancement of the weldability in resistance spot welding. *AWS Detroit Section Sheet Metal Welding Conference IV*, Southfield, Mich.
3. Zhao, Y. Y., Zhang, Y. S., Lai, X. M., and Wang, P.-C. 2013. Resistance spot welding of ultrathin automotive steel. *ASME Journal of Manufacturing Science and Engineering* 135(4): 021012.1–10.
4. Williams, N. T., and Parker, J. D. 2004. Review of resistance spot welding of steel sheets Part 2 Factors influencing electrode life. *International Materials Reviews* 49(2): 77–108.
5. Trommer, G. 2009. Resistance spot welding using continuous tape. *Welding Journal* 88(12): 20-s to 22-s.
6. Stieglbauer, W. 2006. Delta spot — Spot welding with process tape. IIW Doc.III-1381-06.
7. Kolarik, L., Sahul, M., Kolarikova, M., Sahul, M., Turna, M., and Felix, M. 2012. Resistance spot welding of dissimilar steels. *Acta Polytechnica* 52(3): 43–47.
8. Qiu, R. F., Iwamoto, C., and Satonaka, S. 2009. Interfacial microstructure and strength of steel/aluminum alloy joints welded by resistance spot welding with cover plate. *Journal of Materials Processing Technology* 209: 4186–4193.
9. Abdo, A., Harraz, M., Reisgen, U., Schleser, M., and Schiebahn, A. 2013. Resistance spot welding of aluminum alloy 5182 to zinc coated DP600 steel using process tape technique. *International Journal for Scientific Research and Development* 1(10): 2212–2216.
10. Qiu, R. F., Satonaka, S., and Iwamoto, C. 2009. Mechanical properties and microstructures of magnesium alloy AZ31B joint fabricated by resistance spot welding with cover plates. *Science and Technology of Welding and Joining* 14(8): 691–697.
11. Satonaka, S., Iwamoto, C., Murakami, G.-i., and Matsumoto, Y. 2012. Resistance spot welding of magnesium alloy sheets with cover plates. *Welding in the World* 56(7-8): 44–50.
12. American Welding Society. 2012. *Test Methods for Evaluating the Resistance Spot Welding Behavior of Automotive Sheet Steel Materials*. AWS D8.9M:2012.
13. Zhang, X. Q., Chen, G. L., and Zhang, Y. S. 2008. Characteristics of electrode wear in resistance spot welding dual-phase steels. *Materials & Design* 29(1): 279–283.
14. Holliday, R. J., Parker, J. D., and Williams, N. T. 1996. Relative contribution of electrode tip growth mechanism in spot welding zinc coated steels. *Welding in the World* 37(4): 186–193.
15. Dong, S. J., and Zhou, Y. 2003. Effects of TiC composite coating on electrode degradation in microresistance welding of nickel-plated steel. *Metallurgical and Materials Transactions A* 34(7): 1501–1511.
16. Chatterjee, K. L., and Waddell, W. 1996. Electrode wear during spot welding of coated steels. *Welding and Metal Fabrication* 64: 110–114.
17. Chuko, W., and Gould, J. E. 2002. Development of appropriate resistance spot welding practice for transformation-hardened steels — Phase 2: Evaluation of post-weld cooling rate techniques. Report to the American Iron and Steel Institute.
18. Gould, J. E., Khurana, S. P., and Li, T. 2006. Predictions of microstructures when welding automotive advanced high-strength steels. *Welding Journal* 85(5): 111-s to 116-s.
19. *ASM Metals Handbook*. 2001. Desk edition. ASM International.
20. *ASM Metals Handbook*. 1992. Vol. 3, Alloy Phase Diagrams. ASM International.
21. *ASM Specialty Handbook: Copper and Copper Alloys*. 2001. ASM International.